La mer 46 : 37-47, 2008
Société franco-japonaise d'océanographie, Tokyo

Diurnal Tidal Current on the Eastern Shelf of Hidaka Bay —Can juvenile walleye pollock, *Theragra chalcogramma,* move southeastward with the diurnal tidal current?—

Hiroshi KURODA[1)], Yutaka ISODA[2)], Satoshi HONDA[3)], Hidetaka TAKEOKA[4)] and Manabu SHIMIZU[1)]

Abstract: It has been reported that juvenile walleye pollock (age 0) moves southeastward along the eastern shelf of Hidaka Bay, Japan, in the early summer, when the mean flow direction on this shelf is opposite to its movement, i.e., northwestward flow. A hypothesis was previously proposed that the juvenile can move against the mean flow by combining an active diurnal vertical migration with background diurnal tidal currents. A strong vertical shear of the diurnal tidal current is essential for this hypothesis, but the presence has not been clarified. In order to describe characteristics of the diurnal tidal current on the eastern shelf of Hidaka Bay and to argue the validity of this hypothesis, we conducted a mooring current measurement from December 2002 to July 2003 and one-shot/25.8-hour ADCP surveys in the early summer (June) of 2003. It is shown that the O_1 current is by far the largest of the four major tidal constituents, followed by the K_1 current. This magnitude relation is inconsistent with that of the tidal height amplitude, $M_2 > K_1 > O_1 > S_2$. The spatial structure of the O_1 current from the ADCP survey is compared with that from free coastal-trapped wave (CTW) dynamics. As a result, it is indicated that the O_1 tidal height and current are mainly governed by a basin-scale external gravity wave and a first-mode baroclinic CTW with about 100-km wavelength, respectively. The O_1 current related to the CTW exhibits a nearly barotropic structure on the shelf without a strong vertical shear, independent of the seasonal stratification. Consequently, it is concluded that the proposed hypothesis must be quantitatively invalid.

Keywords: *Hidaka Bay, K_1 and O_1 current, CTW, Theragra chalcogramma*

1. Introduction

Hidaka Bay is an open-type bay with U-shaped topography, west of Cape Erimo, in the North Pacific (Fig. 1). In this study the northeastern part of the shelf region of this bay with a straight coastline of 120 km is simply referred to as the eastern shelf. It has been well-known that tidal height fluctuations around this bay are mainly governed by basin-scale external gravity/Kelvin waves from the North Pacific which propagate southwestward along Kuril and Japan Islands (OGURA, 1933). It has been considered that there are spatial differences in characteristics of tidal currents around Hidaka Bay due to topographic effects of Funka Bay (SAKATA and ISODA, 1998) and tidal waves propagating from the Japan Sea through Tsugaru Strait (ODAMAKI, 1984; KURODA *et al.*, 2004). However, the focus of these previous studies is limited to steady-state tidal currents on the western part of Hidaka Bay. Thereby, it is required to understand

1) National Research Institute of Fisheries Science, 2–12–4 Fukuura, Kanazawa, Yokohama, Kanagawa 236–8648, Japan.
2) Graduate School of Fisheries Science, Hokkaido University, 3–1–1 Minato-cho, Hakodate, Hokkaido 041–8611, Japan.
3) Hokkaido National Fisheries Research Institute, 116 Katsurakoi, Kushiro, Hokkaido 085–0802, Japan.
4) Center for Marine Environmental Studies, Ehime University, 2–5 Bunkyo-cho, Matsuyama, Ehime 790–8577, Japan.
* Corresponding author; Hiroshi KURODA
E-mail : kurocan@affrc.go.jp
Tel. +81–45–788–7698/Fax +81–45–788–5001

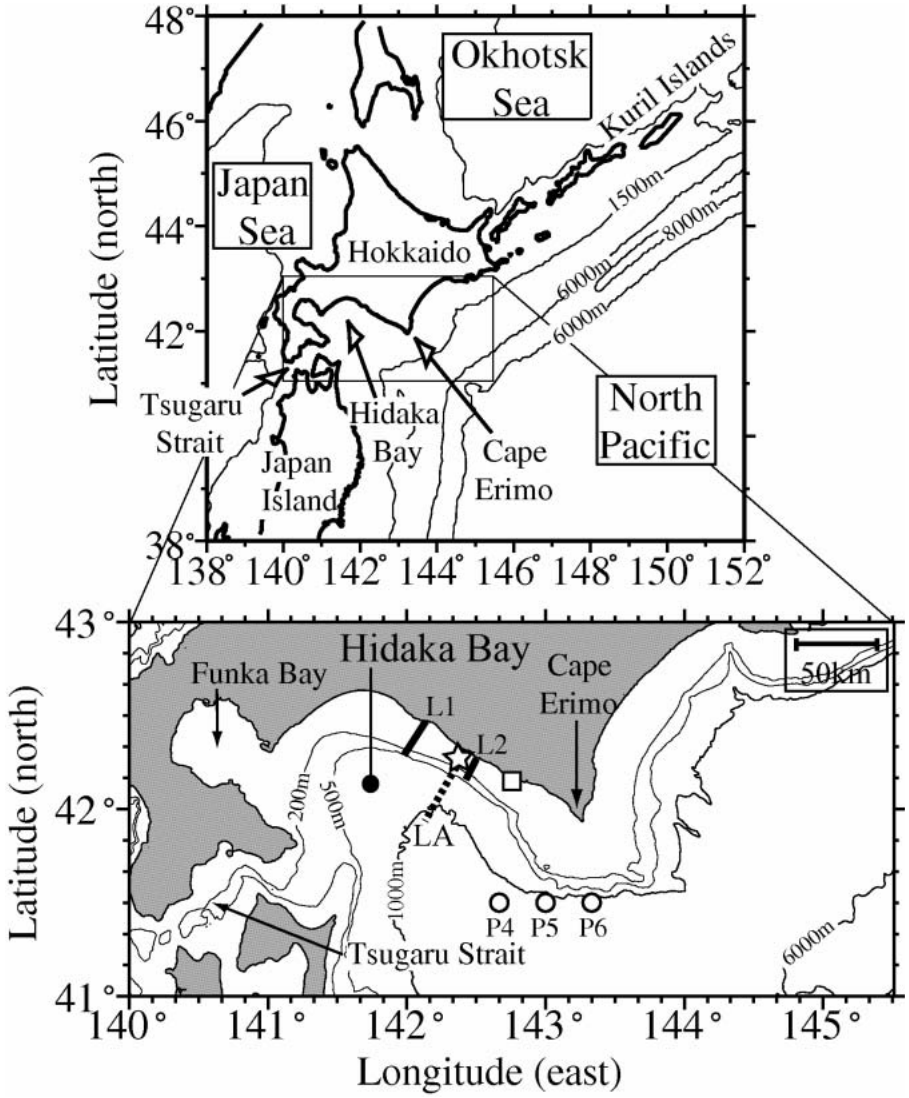

Fig. 1. Bathymetry in and around Hidaka Bay. Star mark, open square and open circle in lower panel denote locations of mooring current site, tide gauge at Urakawa, and CTD stations of P4-P6, respectively. Thick lines along L1 and L2 are transects of 25.8-hour ADCP surveys.

characteristics of the tidal currents on the eastern shelf without neglecting the unsteadiness. In addition, recently, understanding the properties of the diurnal tidal current on this shelf has become an important issue in fisheries science for the following reason.

Fig. 2 (a) illustrates the schematic view of the early life history of walleye pollock (*Theragra chalcogramma*) hatching in winter around the mouth of Funka Bay, the main spawning ground of the Japanese Pacific population of this species (e.g., NISHIMURA *et al.*, 2002). Although a part of larvae and juveniles are transported southward away from the mouth of Funka Bay, the rest of them remains in Funka Bay until May. It has been observed that the juveniles begin to move southeastward on the eastern shelf with water depths less than 100 m at the beginning of summer (June), when they grow to about 50–100 mm in total

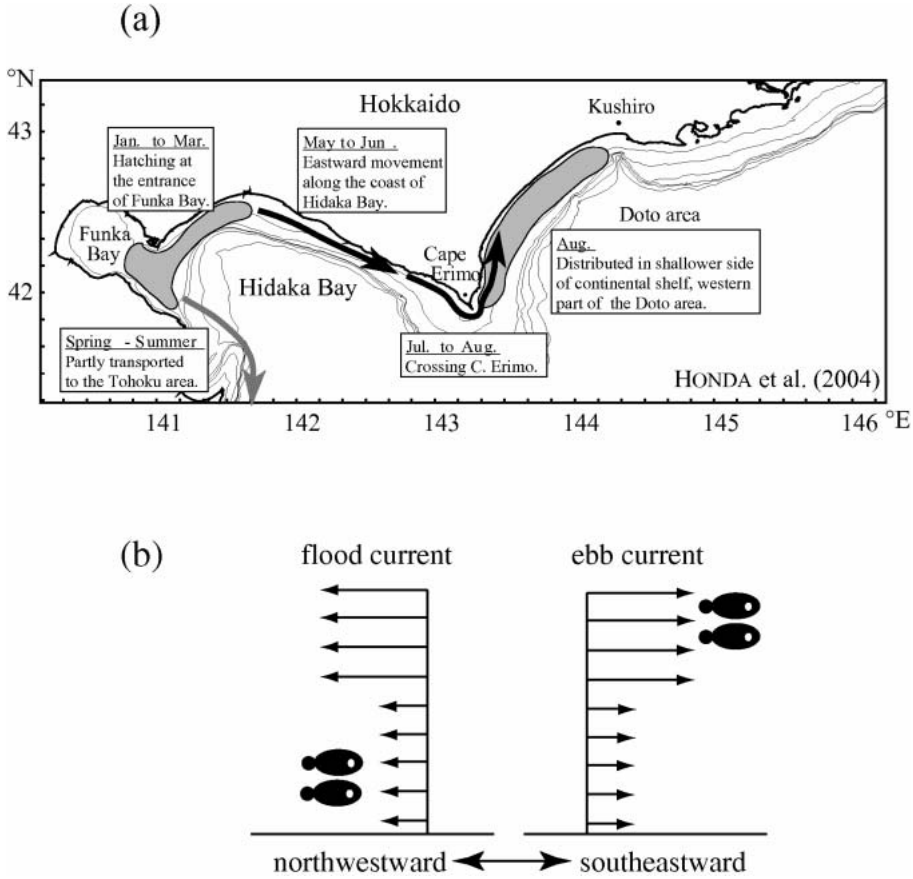

Fig. 2. (a) Early life history of walleye pollock hatching in winter around the mouth of Funka Bay (from HONDA *et al.*, 2004). (b) Schematic view of the DM hypothesis under the two-layer configuration.

length (HONDA *et al.*, 2004). However, the mean current direction on the shelf in this season is opposite to their movement, i.e., northwestward flow (KURODA *et al.*, 2006; ROSA *et al.,* 2007).

This inconsistency was discussed in symposium on Japanese Coastal Oceanography, Sapporo, October 2002 (HONDA *et al.*, 2003). The horizontal swim capability of juvenile pollock was neglected at the symposium because it was unclear. A hypothesis was proposed that juvenile pollock can move against the mean flow by combining an active diurnal vertical migration with background diurnal tidal currents (Fig. 2 (b)), as well as plaice, sole, flounder and shrimp larvae (RIJNSDORP *et al.*, 1985; GRIOCHE *et al.*, 2000; CATTRIJSSE *et al.*, 1997; GIBSON, 2003; MCKEOWN, 1984). In the present study, we refer to this hypothesis as "DM hypothesis". In this hypothesis, juvenile pollock migrates vertically on a diurnal cycle as synchronizing its vertical position with a strong southeastward or a weak northwestward tidal flow (Fig. 2 (b)). A strong vertical shear of the diurnal tidal current associated with bottom friction or internal wave is crucial for the DM hypothesis. However, as mentioned above, the dominance of the diurnal tidal current and the presence of the strong vertical shear have not been understood.

The purpose of this study is twofold: firstly, to describe characteristics of the diurnal tidal current on the eastern shelf on the basis of observation data, and secondly, to discuss the validity of the DM hypothesis. On the eastern shelf of Hidaka Bay, we carried out a mooring

current measurement for about 8 months and one-shot/25.8-hour ADCP surveys in the early summer of 2003 (Section 2). Several interesting features of the diurnal tidal current are detected, which cannot be identified in the western part of Hidaka Bay, e.g., dominance of the O_1 current and high temporal variability of harmonic constant of the K_1 and O_1 current (Section 3). Spatial structures of the O_1 current from the one-shot ADCP survey are compared with those from free coastal-trapped wave dynamics (Section 4) , and the validity of the DM hypothesis is discussed from observational and theoretical results (Section 5). Lastly, several findings from this study are briefly summarized (Section 6).

2. Data and data processing

A mooring current measurement was performed near the coast on the eastern shelf of Hidaka Bay from 20 November 2002 to 26 July 2003 (Fig. 1). An electromagnetic current meter ("compact-EM", Alec Electronics Co., Ltd) was moored at 7 m below the sea surface. This mooring site is about 3 km offshore from the coast, and the water depth is 35 m. The current velocity and direction, averaged over 30 sec., were recorded every two hours. The accuracy of this current meter is 1 cm s^{-1}.

Hourly tide gauge data at Urakawa during the same period of the mooring current measurement were collected from the Japan Oceanographic Data Center (JODC). The sea level data was subsampled every 2 hours to match the sampling time of the current data.

Across-shelf ADCP transects along L1 and L2 (Fig. 1) were repeated back and forth for 25.8 hours on 17 and 16 June 2003, respectively, using the R/V *Kaiyo-maru No.7*. CTD and X CTD observations were carried out before the ADCP measurements. The transit times between the end points of each transect repetition are about 1.5 hours. The ADCP ("CI–30" (130 kHz), Furuno Electric Co., Ltd) was set to sample 3 vertical levels (17, 42 and 67 m). The bottom track-mode current velocity and direction were recorded every 15 seconds. The measurement accuracy of this system is 0.1 kt. ($\sim$5.0 cm s^{-1}). The original ADCP data were separated into several stations on L1 and L2, and averaged for each transect.

For a theoretical calculation in Section 4, a density profile of 0–1000 m on the eastern shelf in June 2003 was prepared by merging CTD and XCTD data. All the CTD and XCTD profiles measured on L1 and L2 were averaged for each depth. However, the maximum depth of the mean density profile is limited to about 500 m. To extrapolate a density profile at depths greater than 500 m, we used 1-m pitch CTD data at three stations of P4-P6 (Fig. 1), obtained on 2 May 2003 by the Japan Meteorological Agency (JMA). The density profiles at 500–1000 m were averaged over P4-P6 for each depth, and then combined with the mean density profile of 0–500 m from L1 and L2.

3. Characteristics of observed tidal current

3.1. Mooring current measurement

Using the mooring current and tide gauge data during the entire mooring period, harmonic analysis for the four major tidal constituents (K_1, O_1, M_2 and S_2) was conducted. The current ellipses are shown in Fig. 3, and the harmonic constants are listed in Table 1. It is found that the O_1 current is by far the most dominant, the major-axis amplitude of which is

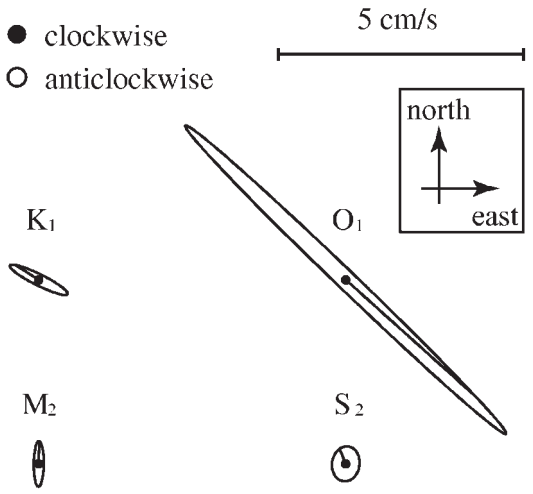

Fig. 3. Current ellipses of the four major tidal constituents, estimated from the entire mooring period from December 2002 to July 2003. Phase is denoted by straight line connecting each elliptic curve with its center, and the rotational direction of all tidal constituents is clockwise, as represented by closed circle.

4.5 cm s^{-1}. The O_1 current oscillates clockwisely and rectilinearly along the northwest-southeast coastline. On the other hand, the major-axis amplitude of another constituent is less than the current meter accuracy of 1 cm s^{-1}. The major-axis directions of the M_2 and S_2 current are not parallel to the coastline and the shapes of M_2 and S_2 current ellipse are clearly different regardless of their similar periods, implying that the semi-diurnal current signals are contaminated by a non-tidal noise component.

Compared with MSA (1983), the harmonic constants of tidal height at Urakawa (Table 1) are almost consistent with those along the Pacific coast of Hokkaido (not shown) since the tidal height fluctuations along the coast are mainly governed by basin-scale external gravity/Kelvin waves (OGURA, 1933). The magnitude relation of the tidal height amplitude ($M_2 > K_1 > O_1 > S_2$) is clearly different from that of the tidal current amplitude ($O_1 >> K_1 \sim M_2 \sim S_2$). This suggests that a non-divergent wave, such as Rossby and internal wave, contributes to the O_1 current on the eastern shelf of Hidaka Bay.

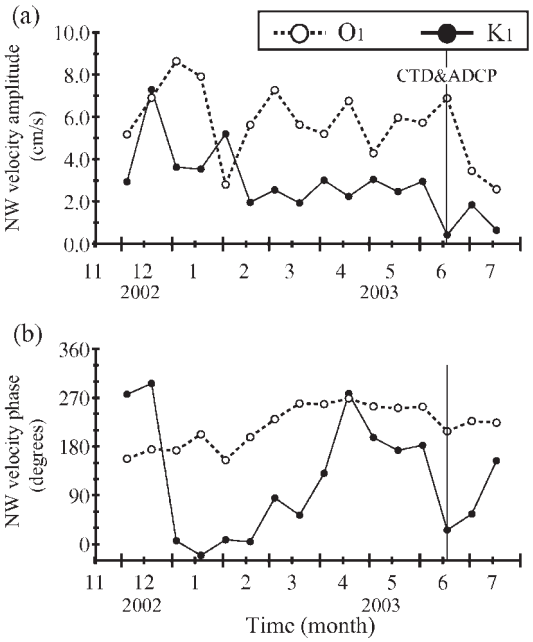

Fig. 4. Temporal variations of (a) amplitude and (b) phase for northwest component of the K_1 and O_1 current. Vertical straight line indicates the time of 17 June 2003, around which ADCP and CTD observations were conducted on L1 and L2.

To examine the temporal variability of harmonic constant of the K_1 and O_1 current, the original current time series was divided into subseries with a length of 15 days. Harmonic analysis for the four major tidal constituents was sequentially conducted for each subseries. Fig. 4 shows the time series of diurnal amplitude and phase for the northwest velocity component. The amplitude of the K_1 (O_1) current varies dramatically with time from 0.4 to 7.3 cm s^{-1} (from 2.6 to 8.6 cm s^{-1}) (Fig. 4 (a)). The amplitude of the O_1 current exceeds that of the K_1 current, except for two cases in December and February. The K_1 and O_1 current phases also vary drastically (Fig. 4 (b)) and, the variability of the K_1 phase seems higher. It is inferred that the extremely small amplitude of the K_1 current of 0.7 cm s^{-1} from the about 8-month data (Fig. 3) is partly attributed to this higher variability of the K_1 phase. The M_2 and S_2 current amplitudes also change between 0.5 and 1.5 cm s^{-1} (not shown), close to the current meter accuracy of 1 cm s^{-1}.

To check the influence of the P_1 current on the seasonal variability of the K_1 current (Fig. 4), a harmonic analysis for the K_1, O_1, M_2, S_2 and P_1 constituents was sequentially applied to the 15-day subseries under the assumption of a

Table 1. Harmonic constants of tidal height at Urakawa and tidal current at the mooring site estimated from time series from December 2002 to July 2003.

		M_2	S_2	K_1	O_1
Tidal Current (mooring site)	Major-axis direction (degrees)	1	8	296	314
	Major-axis amplitude (cm/s)	0.5	0.4	0.7	4.5
	Major-axis phase (degrees)	350	33	328	217
Tidal Level (Urakawa)	amplitude (cm)	29.9	12.9	26.4	21.7
	phase (degrees)	107.3	149.2	167.6	152.4

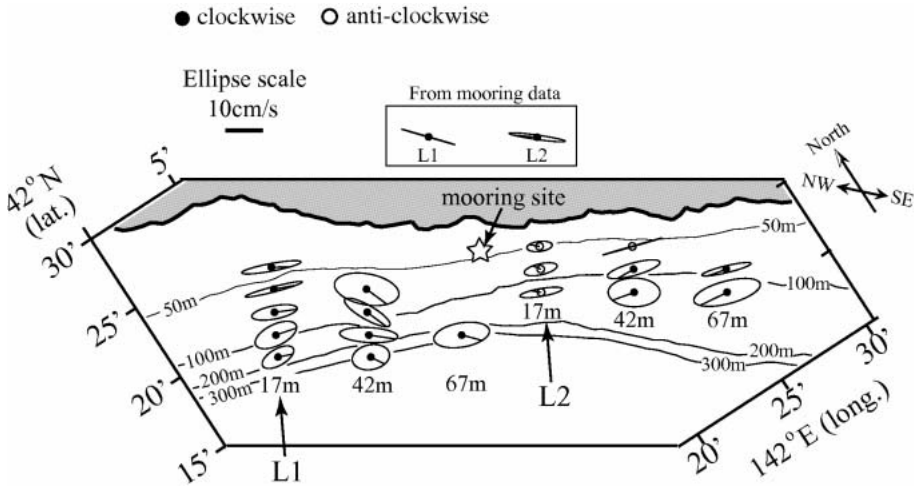

Fig. 5. Diurnal current ellipses from ADCP surveys in June 16th (L2) and 17th (L1) 2003. Location of ADCP stations is consistent with the center position of current ellipses at 17 m, in the right position of which current ellipses at 42 m and 67 m are plotted.

Table 2. Diurnal current phases for the major-axis component from 25.8-hour ADCP survey and 26-hour mooring current record. Numeral in parenthesis indicates the phase difference from a mean phase on each transect. Reference time of phase is 2000/1/1 00：00：00JST.

		7m	17m	42m	67m
ADCP (L1) 2003/6/17	L1–1	–	127.6 (−18.5)	–	–
	L1–2	–	139.6 (−6.5)	134.0 (−12.1)	–
	L1–3	–	170.4 (24.3)	156.5 (10.4)	–
	L1–4	–	164.0 (17.9)	160.3 (14.2)	133.2 (−12.9)
	L1–5	–	144.7 (−1.4)	130.4 (−15.7)	–
ADCP (L2) 2003/6/16	L2–1	–	37.6 (−7.5)	43.3 (−1.8)	–
	L2–2	–	65.8 (20.7)	48.7 (3.6)	38.7 (−6.4)
	L2–3	–	62.3 (17.2)	33.5 (−11.6)	30.7 (−14.4)
mooring	Mooring 2003/6/16	31.6	—	–	–
	Mooring 2003/6/17	59.6	—	–	–

phase reference： 2000/01/01 00：00：00JST

constant amplitude ratio (0.326) and phase difference (357.3 degrees) between the K_1 and P_1 constituents (ODAMAKI, 1989), based on the harmonic constant of the tidal height at Urakawa (MSA, 1983). It was found that the maximum difference of amplitude and phase from Fig. 4 is 1.7 cm s^{-1} and 19 degrees, respectively, but the time variation pattern is similar to that of Fig. 4. It is suggested that the influence of the P_1 current is negligible for the seasonal variability of the K_1 current.

Here, we focus on the K_1 and O_1 current amplitudes plotted at 16 June 2003 in Fig. 4 (a), when the 25.8-hour ADCP surveys were performed. It is found that the K_1 current amplitude (0.42 cm s^{-1}) is much smaller than the O_1 current amplitude (6.9 cm s^{-1}). These diurnal amplitudes were computed from a subseries between 9 June and 24 June under the assumption of constant amplitude and phase for the 15 days. If this assumption is valid, at least, for this subseries, the diurnal current captured by the ADCP surveys depends primarily on the O_1 current.

3.2. 25.8-hour ADCP measurement

Using not only the 25.8-hour ADCP data along L1 and L2 but also the mooring current data for 26 hours corresponding to each ADCP-observation period, the diurnal, semi-diurnal

and residual components were decomposed by harmonic analysis (e.g., CÁCERES *et al.*, 2002). The residual northwestward flow, nearly barotropic, was described in KURODA *et al.* (2006). The diurnal current ellipses and major-axis phases based on 1 January 2000 00:00:00 JST (not the same as the lag of tide in Table 1 and Figs. 3,4 (b)) are shown in Fig. 5 and listed in Table 2, respectively. In Fig. 5, the center position of the current ellipses at 17 m on L1 and L2 corresponds to the actual position of ADCP stations, and the upper two ellipses surrounded by a solid square are from the 26-hour mooring current record.

The major-axis direction of the current ellipse tends to be parallel to the coastline. Clockwise rotations are dominant except for at 17 m on L2. Major-axis amplitudes from the ADCP survey are in a range of 4 cm s^{-1} to 11 cm s^{-1}, comparable to the major-axis amplitude of about 9 cm s^{-1} from the 26-hour mooring current data. In this regard, however, it should be noted that quantitatively accurate discussion for the diurnal current estimated from the ADCP survey may be difficult because of the ADCP system accuracy of about 5 cm s^{-1}.

The major-axis amplitude based on the 26-hour mooring current record (9.0 cm s^{-1}) (Fig. 5) is closer to the O_1 current amplitude (6.9cm s^{-1}) at 16 June 2003 in Fig. 4 (a) than the K_1 current amplitude (0.42 cm s^{-1}). Here we assume that the diurnal current in Fig. 5 is the O_1 current. Under this assumption, the phase listed in Table 2 can be converted to the lag of the O_1 tide, the same as in Table 1 and Figs. 3,4 (b), by adding 154.18 degrees. The converted phases for the 26-hour mooring data and ADCP data on L2 are in a range of 184.9 to 220 degrees, almost consistent with the O_1 phase of 210 degrees plotted at 16 June 2003 in Fig. 4 (b). Accordingly, it is indicated that the diurnal current recorded by the ADCP survey mainly depends on the O_1 current.

Numerals in parenthesis of Table 2 are phase deviations from a mean value on each transect. The phase deviations for L1 and L2 are in a range of −18.5 to 24.3 degrees and −14.4 to 20.7 degrees, respectively. This indicates that the diurnal current is in phase for the vertical and across-shelf direction within an error range of ±25 degrees. A systematic phase difference is detected between L1 and L2 (Table 2). The current phase on L2 remarkably leads that on L1, indicating that a tidal wave related to the observed diurnal current propagates northwestward. The major-axis current phases averaged over L1 and L2 are 146.1 and 45.1 degrees, respectively. That is, the mean phase lag (L1 minus L2) is 101 degrees. A wavelength of 107 km is estimated from the mean phase lag and distance of 30 km between L1 and L2, if the wavelength is longer than the 30 km. This wavelength is much smaller than the spatial scale ($O(10^4$ km)) of the external gravity waves, governing tidal height fluctuations, by two orders of magnitude.

Since the O_1 frequency is subinertial at the mooring site on the shelf near the coast, one possible interpretation for the wave characteristics captured by the ADCP survey is that the dominant O_1 current is controlled mainly by coastal-trapped waves (CTWs). The CTWs generally exhibit a 100-km order of wavelength and weak divergence (e.g., WANG and MOORES, 1976), which seem to be able to explain our observational results. To confirm this possibility, the free CTWs' properties are theoretically investigated in the next section.

4. Free coastal-trapped wave dynamics

The dispersion curve and mode structure of free baroclinic CTWs are computed under a given density stratification and topographic condition. A set of linearized, inviscosity, and f-plane equations are solved by using a numerical technique in WANG and MOORES (1976), DALE and SHERWIN (1996), and ZOAKOS *et al.* (2004). An idealized configuration is designed in the Cartesian coordinate of (x, y, z). A straight coastline along the y-axis direction is assumed at x=0. The positive directions of x, y and z are defined as the offshore direction, the direction toward which Kelvin waves propagate, and the upward direction, respectively. Two input variables required for this model are the bottom topography h (x) and Brunt-Väis älä frequency N (z), which are the functions of x and z alone, respectively.

The main solved equation is

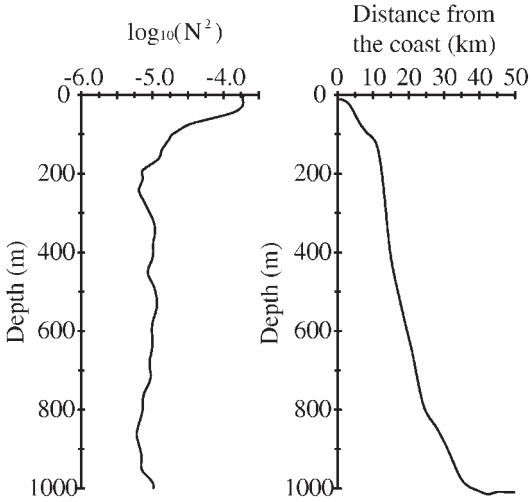

Fig. 6. Brunt-Väisälä frequency based on density profile processed in Section 2 (left panel) and bottom topography along LA seen in Fig. 1 (right panel).

$$\left[p_{xx}+p_{yy}+f^2\left(\frac{p_z}{N^2}\right)_z+\left(\frac{p_z}{N^2}\right)_{ztt}\right]_t=0, \quad (1)$$

where subscript denotes the partial differential, p is the pressure perturbation, and f is the Coriolis parameter. The boundary conditions at the sea surface, sea bottom, coast, and infinite offshore are

$$p_{zt}+N^2g^{-1}p_t=0 \text{ at } z=0, \quad (2)$$

$$f^2p_{zt}+p_{ztt}+N^2h_x\,(p_{xt}+fp_y)=0 \text{ at } z=-h\ (\mathrm{x}), \quad (3)$$

$$p_{xt}+fp_y=0 \text{ at } x=0, \quad (4)$$

and

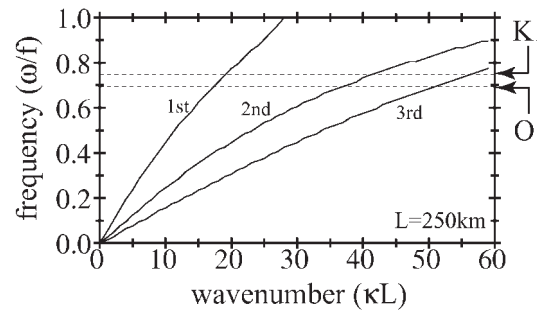

Fig. 7. Dispersion curves of the first-mode to third-mode CTWs.

$$p\to 0 \text{ at } x\to\infty, \quad (5)$$

respectively. Equations (2), (3), (4) and (5) represent the free sea surface, no normal flows to the sea bottom and coast, and coastal trapping, respectively.

Equations (1) to (5) in the z coordinate are converted to those in the σ coordinate. The following wave solution is substituted into Eqs. (1) to (5),

$$p\,(x,\,y,\,\sigma)=\hat{p}\,(x,\,\sigma)e^{i(\omega t+ly)},$$

where ω and l are the angular frequency and alongshore wavenumber, respectively. This wave form is almost consistent with the observation, i.e., the O_1 current is in phase for the vertical and across-shelf direction within an error range of ± 25 degrees (Table 2). One-km horizontal grid, evenly spaced 75-sigma levels,

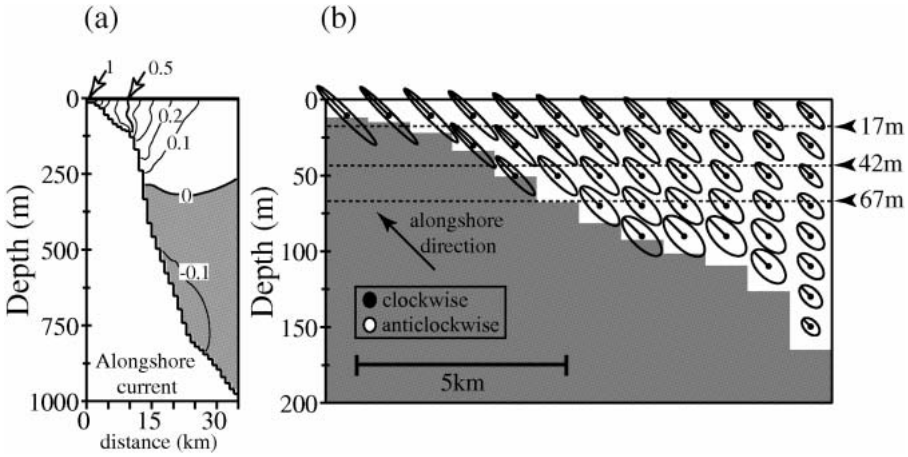

Fig. 8. Vertical sections of (a) alongshore velocity normalized by the maximum value at the coast and (b) current ellipse on the shelf, for the first-mode CTW with the O_1 frequency.

and the Coriolis parameter at 42 ($=9.73\times10^{-5}$ s^{-1}) are adapted. The bottom topography along LA (see Fig. 1) and Brunt-Väisälä frequency based on the density profile processed in Section 2, shown in Fig. 6, are given for the calculation. A set of equations of $\hat{p}$ are solved by using a resonance response.

Fig. 7 shows dispersion curves of the first-mode to third-mode CTWs. It is found that the CTWs can be permitted at both the K_1 and O_1 frequencies. The wavelengths of first- to third-mode CTW for the O_1 frequency are 92 km, 42 km and 30 km, respectively. The first-mode wavelength is closest to the wavelength of 107 km estimated from the ADCP survey.

Fig. 8 (a) shows the vertical section of the normalized alongshore velocity for the first-mode CTW with the O_1 frequency. The node (0-value curve) extends along the depth of 300 m from the sea bottom just offshore the shelf edge. This indicates that the alongshore velocity is vertically in phase on the shelf and out of phase on the slope. To focus on current structures near the coast, the O_1 current ellipses on the shelf derived from the first-mode CTWs are shown in Fig. 8 (b). The O_1 current seems nearly barotropic on the shelf. Compared between Fig. 5 and Fig. 8 (b), the theoretical and observed ellipses are not quantitatively consistent with each other because of the ADCP system accuracy and some idealizations of the theoretical model, but several features are qualitatively consistent. The clockwise rotation is dominant on the shelf in the theoretical result (Fig. 8 (b)) as well as the observed result (Fig. 5). In Fig. 8 (b), the current ellipse near the coast is rectilinear and parallel to the coastline, and the ellipses around the depth of 17 m gradually approach a circular shape toward the offshore direction. This across-shelf feature is especially notable at 17 m along L1 (Fig. 5). Moreover, for the first-mode CTW with the O_1 frequency, the theoretical ratio of the alongshore current amplitude to the sea-level amplitude at the coast is estimated as 10 s^{-1}. This value indicates that the CTW is weakly divergent, as expected from Table 1. Consequently, it is concluded that the O_1 current observed in June 2003 is mainly governed by the first-mode baroclinic CTW.

5. Discussion

In this section we discuss the validity of the DM hypothesis under the two-layer configuration (Fig. 2 (b)) for the shelf with water depths less than 100 m, where juvenile pollock was in fact detected during our survey of L1 and L2 (HONDA, personal communication). Moreover, the tidal current selectivity to optimally move southeastward is explicitly given for juvenile pollock although the purpose of the juvenile migration may be to prey on zooplankton migrating vertically on day-and-night cycle (HONDA *et al.*, 2004).

Upper- and lower-layer diurnal tidal currents are assumed to be either in phase or out of phase. The amplitudes of southeast velocity component in the upper and lower layer are given as U_1 (>0) and U_2, respectively ($U_2>0$ ($U_2<0$) means that the upper and lower currents are in phase (out of phase)). Under the assumption of the tidal current selectivity, juvenile pollock stays in the upper (lower) layer when the upper layer exhibits the southeastward (northwestward) flow. In this case the southeastward moving speed of juvenile pollock averaged over a diurnal cycle is

$$\frac{\omega}{2\pi}\left[\int_0^{\pi/\omega} U_1 \sin\omega t \; dt + \int_{\pi/\omega}^{2\pi/\omega} U_2 \sin\omega t \; dt\right] = (U_1 - U_2)/\pi ,$$

where ω is the diurnal angular frequency. Moreover, since a northwestward mean flow (U_{mean} (<0)), nearly barotropic, was observed on the eastern shelf in the early summer of 2003 (KURODA *et al.*, 2006), the above moving speed is modified as $(U_1-U_2)/\pi + U_{mean}$. The southeastward movement of the juvenile is feasible for $(U_1-U_2)/\pi + U_{mean}>0$. The actual values of U_1 and U_{mean} are approximately 8 cm s^{-1} (Fig. 5) and -7.5 cm s^{-1}, respectively (the latter is the alongshore velocity of the mooring current data averaged over June and July 2003). The relation of $U_2<-16$ cm s^{-1} is derived, indicating that the strong shear flow out of phase between the upper and lower layer is required for the DM hypothesis.

However, as mentioned above, such an intense vertical shear was not observed and theoretically supported (Figs. 5,8). The strong shear should not be also theoretically explain-

able even if the bottom friction is added to the free CTW dynamics. This is because the diurnal time scale is too short for the friction to efficiently reduce/modify an alongshore barotropic current on the shelf (CHAPMAN and BRINK, 1987). As a result, it is concluded that the DM hypothesis must be quantitatively invalid.

Moreover, this conclusion implies that juvenile pollock can actively swim horizontally/southeastward against the mean flow. For the mean flow of the -7.5 cm s^{-1} near the coast (U_{mean}), if the juvenile is able to swim with a mean speed of 12 cm s^{-1}, it can move from the mouth of Funka Bay to Cape Erimo (120km) in a month. The swim speed of 12 cm s^{-1} may be reasonable according to a recent experiment of HURST (2007), which reported that the routine and maximum swim speeds of an 80 mm juvenile walleye pollock are in a range of 6 cm s^{-1} to 8 cm s^{-1} and of 22 cm s^{-1} to 31 cm s^{-1}, respectively.

6. Conclusions

To describe characteristics of the diurnal tidal current on the eastern shelf of Hidaka Bay and argue the validity of the DM hypothesis, we carried out a mooring current measurement from December 2002 to July 2003 and one-shot/25.8-hour ADCP surveys in June 2003. It was shown that the O_1 current is by far the largest of the four major tidal constituents, whereas the O_1 tidal height is the third largest. The harmonic constant of the K_1 and O_1 current changes dramatically with time. The spatial structure of the O_1 current from the ADCP survey was compared with that estimated from the free CTW dynamics. As a result, it was indicated that the O_1 tidal height and current on this shelf are mainly governed by a basin-scale external gravity/Kelvin wave and a first-mode baroclinic CTW, respectively. The O_1 current depending on the CTWs showed the nearly barotropic structure on the shelf without a strong vertical shear, independent of the seasonal density stratification. Therefore, the DM hypothesis must be invalid, implying that juvenile pollock is able to actively swim southeastward against the mean flow. This may also be supported by recent swim experiments performed by HURST (2007).

Lastly, we remark a few dynamical issues which require clarification in future work. Two observed features in Fig. 4 seem very intriguing; one is the amplitude difference between the K_1 and O_1 currents, the other is the high temporal variability of the harmonic constant (i.e., amplitude and phase) of the K_1 and O_1 currents. In particular, for the latter point, many possible causes can be supposed, such as temporal changes of CTWs' generation, propagation, scattering, and damping process due to the change of density stratification (e.g., WILKIN and CHAPMAN, 1990; BRINK, 2006). However, since the present study is based on only one mooring current measurement and one-shot ADCP surveys restricted to June 2003, it is not possible to comprehend a spatial structure of the K_1 and O_1 tidal currents over the eastern shelf throughout the entire of the mooring period. Hence, to clarify these issues, as one of the subsequent steps, it is probably effective to examine temporal and spatial variation of the diurnal CTWs on the eastern shelf by deploying plural mooring current meters.

Acknowledgements

We are deeply indebted to the captain, officers and crew of the R/V *Kaiyo-maru No. 7* for hydrographic observations on L1 and L2. We wish to express our sincere thanks to Mr. CHIMOTO and other member in the Federation of Fisheries Cooperative Association of Shizunai, who helped us to set and recovery the mooring current meter. We would like to thank the member of the National Research Institute of Fisheries Science for patient support and encouragement. We also thank the JODC for tide gauge data at Urakawa, and the Japan Metrological Agency for CTD data along PH Line (41° 30'N). Thanks are extended to the editor and two anonymous reviewers for helpful and constructive comments. Finally, this work was supported by a Grant-in-Aid for JSPS Fellows.

References

BRINK, K.H. (2006): Coastal-trapped waves with finite bottom friction. Dynamics of Atmospheres and Oceans, **41**, 171–190.

CÁCERES, M., A. VALLE-LEVINSON, H.H. SEPÚLVEDA and K. HOLDERIED (2002): Transverse variability of flow and density in a Chilean fjord. Continental Shelf Research, **22**, 1683–1698.

CATTRIJSSE, A., H.R. DANKWA and J. MEES (1997): Nursery function of an estuarine tidal marsh for the brown shrimp *Crangon crangon*. Journal of Sea Research, **38**, 109–121.

CHAPMAN, D.C. and K.H. BRINK (1987): Shelf and slope circulation induced by fluctuating offshore forcing. Journal of Geophysical Research, **92**, 11741–11760.

DALE, C.A. and T.J. SHERWIN (1996): The extension of baroclinic coastal-trapped wave theory to superinertial frequencies. Journal of Physical Oceanography, **26**, 2305–2315.

GIBSON, R.N. (2003): Go with the flow: tidal migration in marine animals. Hydrobiologia, **503**, 153–161.

GRIOCHE, A., X. HARLAY, P. KOUBBI and L. FRAGA LAGO (2000): Vertical migrations of fish larvae: Eulerian and Lagrangian observations in the Eastern English Channel. Journal Plankton Research, **22**, 1813–1828.

HONDA, S., O. SHIDA and O. YAMAMURA (2003): Life history of walleye pollock, *Theragra chalcogramma*, in the Coastal Oyashio region of Hokkaido. Bulletin of Coastal Oceanography, **41**, 39–47 (in Japanese with English abstract).

HONDA, S., T. OSHIMA, A. NISHIMURA and T. HATTORI (2004): Movement of juvenile walleye pollock, *Theragra chalcogramma*, from a spawning ground to a nursery ground along the Pacific coast of Hokkaido, Japan. Fisheries Oceanography, **13**, 84–98.

HURST, T.P. (2007): Thermal effects on behavior of juvenile walleye pollock (*Theragra chalcogramma*): implications for energetic and food web models. Canadian Journal of Fisheries and Aquatic Science, **64**, 449–457.

KURODA, H., Y. ISODA, M. OHNISHI, M. IWAHASHI, C. SATOH, T. ITO, T. NAKAYAMA, K. ISEDA, K. NISHIZAWA, S. SHIMA and O. TOGAWA, (2004): Examination of harmonic analysis methods using semi-regular sampling data from an ADCP installed on a regular ferry. Oceanography in Japan, **13**, 553–564 (in Japanese with English abstract).

KURODA, H., Y. ISODA, H. TAKEOKA and S. HONDA (2006): Coastal current on the eastern shelf of Hidaka Bay. Journal of Oceanography, **62**, 731–744.

MARITIME SAFTY AGENCY (1983): Table of tidal harmonic constants. 172pp.

MCKEOWN, B.A. (1984): Orientation. In: MCKEOWN, B.A. (Ed.), Fish Migration, Croom Helm, London, 58–86.

NISHIMURA, A., T. HAMATSU, K. YABUKI and O. SHIDA (2002): Recruitment fluctuations and biological responses of walleye pollock in the pacific coast of Hokkaido. Fisheries Science, **68**, 206–209.

ODAMAKI, M. (1984): Tide and tidal current in Tsugaru Strait. Bulletin of Coastal Oceanography, **22**, 12–21 (in Japanese).

ODAMAKI, M. (1989): Tides and tidal currents in the Tsushima Strait. Journal Oceanography Society of Japan, **45**, 65–82.

OGURA, S. (1933): The tides in the seas adjacent to Japan. The Bulletin of the Hydrographic Department, **7**, 1–189.

RIJNSDORP, A.D., M. STRALEN and H.W. VAN DER VEER (1985): Selective tidal transport of North Sea plaice larvae *Pleuronectes platessa* in coastal nursery areas. Transactions of the American Fisheries Society **114**, 461–470.

ROSA, L.A., Y. ISODA, K. UEHARA and T. AIKI (2007): Seasonal variations of water system distribution and flow patterns in the southern sea area of Hokkaido, Japan. Journal of Oceanography, **63**, 573–588.

SAKATA, Y. and Y. ISODA (1998): A numerical model of tides and tidal currents around Funka Bay. Bulletin of the Faculty of Fisheries, Hokkaido University, **49**, 51–57 (in Japanese with English abstract).

WANG, D.-P. and C.N.K. MOOERS (1976): Coastal-trapped waves in a continuously stratified ocean. Journal of Physical Oceanography, **6**, 853–863.

WILKIN, L.J. and D.C. CHAPMAN (1990): Scattering of coastal-trapped waves by irregularities in coastline and topography. Journal of Physical Oceanography, **20**, 396–421.

ZOAKOS, S., P. DYKE and D. GRAHAM (2004): Frictional effects on trapped shelf waves. Ocean Dynamics, **54**, 243–249.

Received March 5, 2008
Accepted August 20, 2008